Journal of Sol-Gel Science and Technology (2024) 112:127–139
https://doi.org/10.1007/s10971-024-06518-2

ORIGINAL PAPER

In-situ acid catalysis strategy to achieve rapid ambient pressure drying preparation of aerogels

Zun Zhao[1] · Yuelei Pan[1] · Mingyuan Yan[1] · Yueyue Xiao[1] · Hui Yang[1] · Xudong Cheng[1]

Received: 28 May 2024 / Accepted: 11 August 2024 / Published online: 16 August 2024

Abstract

Aerogel possesses distinctive features rendering it widely applicable in thermal insulation. Nevertheless, supercritical fluid drying (SCFD) method and freeze-drying employed for aerogels necessitates the complex process, resulting in heightened energy consumption and more risk. To achieve the cost-effective preparation of silica aerogel, we introduce an in-situ acid catalysis strategy for rapidly crafting high-performance SiO_2 aerogel materials under ambient conditions. The resultant SiO_2 aerogels exhibit remarkable porosity (95%) and a substantial specific surface area (759 m^2/g). Furthermore, SiO_2 aerogel composites display low thermal conductivity (0.015 $W \cdot m^{-1} K^{-1}$), coupled with commendable mechanical property. More importantly, we reveal the mechanism of the in-situ acid catalysis (ISAC) strategy. The entire production cycle of SiO_2 aerogel composites and powder is only 6 and 4 h respectively, which greatly reduces the preparation time while ensuring excellent performances. This study introduces a novel approach for the industrial, low-cost, and rapid preparation of SiO_2 aerogel materials through ambient pressure drying.

Graphical Abstract

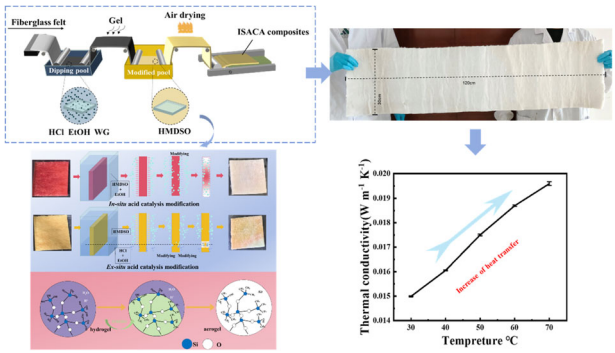

Keywords Aerogels · Ambient pressure drying · In-situ · Acid catalysis strategy

Highlights

- For the first time, the creation of SiO_2 aerogels using in-situ acid catalysis (ISAC) strategy is suggested.
- Reveal the mechanism of the ISAC strategy.
- The entire production cycle of SiO_2 aerogel composites and powder is only 6 and 4 h respectively, which greatly reduces the preparation time.
- The composites have low thermal conductivity (0.015 $W \cdot m^{-1} K^{-1}$) and outstanding mechanical characteristics.

✉ Yuelei Pan
panyl@ustc.edu.cn

✉ Xudong Cheng
chengxd@ustc.edu.cn

[1] State Key Laboratory of Fire Science, University of Science and Technology of China, Hefei 230027 Anhui, PR China

1 Introduction

Aerogels have a highly porous microstructure with an air volume of 85–99.8% [1–3], with a nacre chain network composed of loosely stacked and bonded particles or fibers [4, 5]. Due to these structural characteristics, silica aerogels exhibit low density (typically 30–180 mg cm^{-3}), low refractive index (1.0–1.05), high surface area (500–1200 m^2 g^{-1}), and high mesopore volume (1–5 cm^3 g^{-1}) [6–8]. One of the major characteristics of silica aerogels is their very low thermal conductivity, typically of the order of 0.01 W m^{-1} K^{-1} at ambient temperature, pressure, and relative humidity. These values are significantly lower than the conductivity of air under the same conditions, e.g., 0.025 W m^{-1} K^{-1}. Thus, silica aerogels are among the best-known thermal insulating materials [9].

In the process of preparation of SiO_2 aerogels, the drying is a key step in the transition from wet gel to dry gel. There are three kinds of commonly used drying methods: supercritical fluid drying (SCFD), freeze-drying and ambient pressure drying (APD). SCFD, which is the earliest proposed and most widely used drying method, involves placing the wet gel and solvent in a high-pressure container [10, 11]. The pressure and temperature are adjusted to exceed the corresponding critical point of the solvent, rendering it in a supercritical state. The solvent is then maintained in this state for a period of time before slowly returning it to normal temperature and pressure conditions. During the drying process, the aerogel does not lose its structure due to the absence of a distinct gas-liquid phase differentiation caused by surface tension [12]. Currently SCFD used in industrial production are EtOH supercritical drying and CO_2 supercritical drying. In EtOH supercritical drying process, the temperature will exceed 260 °C and the pressure will reach 6.3 MPa. The supercritical point of CO_2 is 31 °C and 7.29 MPa. Therefore, the SCFD is considerably costly and risky.

Different from SCFD, freeze-drying is a method which converting liquid-gas interface to solid-gas interface under low temperature and low-pressure conditions. This method utilizes the sublimation of solvent in wet gel to avoid the effect of the capillary stresses [13]. The structural control and performance enhancement of aerogels can be realized by freeze-drying. This method is considered as a green and inexpensive drying method [14]. However, the freeze-drying method is too complex to be applied in large-scale industrial production at present.

The fundamental principle of APD involves initially treating the gel to mitigate capillary force. Common treatment methods include aging to reinforce the gel structure, surface modification using silane coupling agents, and substituting high surface tension solvents in the gel pores with low surface tension alternatives. This approach effectively removes the solvent from the nanopores under normal pressure, while preventing the collapse of the nanopores [15, 16]. The traditional APD method to preparing SiO_2 aerogel composites includes: sol–gel synthesis, ion exchange, ageing, solvent replacement, hydrophobic modification and drying. It usually takes 1–7 days to prepare aerogel composites by traditional methods because of the process of solvent replacement and ion exchange. Simultaneously, they possess a relatively high thermal conductivity (0.021–0.049 W m^{-1} K^{-1}) [17–22].

Herein, for the first time, we present an innovative in-situ acid catalysis (ISAC) strategy for achieving the rapid ambient drying preparation of aerogels. Its production equipment is simple. The process is relatively safe because all of the reaction takes place at ambient pressure. Compared with traditional ambient drying, the process of solvent replacement and ion exchange are avoided in this work. The entire production cycle of SiO_2 aerogel composites (120*30 cm^2) and powder is only 6 and 4 h respectively. The thermal conductivity of the in-situ acid catalysis aerogel (ISACA) composites is 0.015 W m^{-1} K^{-1} at room temperature. This is a great improvement compared to previous methods. Additionally, ISAC strategy is less costly and more environmentally friendly. Using water-glass as the silicon source, an inorganic compound, substantially reduces the cost of industrial production while minimizing the consumption of organic solvents (Comparison of different fabrication methods of aerogel composites in Supplementary Table S1).

2 Experimental section

2.1 Materials

Glass-fiber felts were purchased locally from Taobao. Water glass (wt:35%, Na_2O:SiO_2 = 1:3.3) used was purchased from Jiashan Yourui Refractory Co., LTD. Anhydrous alcohol (EtOH, 99%), hydrochloric acid (HCl, AR, 36.0–38.0%) and hexamethyldisiloxane (HMDSO) were obtained from Shanghai Aladdin Biochemical Technology Co., ltd., all analytical pure. The water used in the preparation process is deionized water.

2.2 Preparation of ISACA powder

Initially, 24–82 ml of deionized water, 60 ml of anhydrous ethanol and 58–116 ml of HCl (11.9 mol/L) were added to the beaker and mixed well. Besides, 100 ml of water glass diluent (water glass: deionized water = 1:1, 0.88 mol/L) was added under vigorous stirring. The gel formed in 3–130 min. And then put the gel in 65 °C water bath pot aging for 1 h. Subsequently, 600 ml of hydrophobic modifier was added to

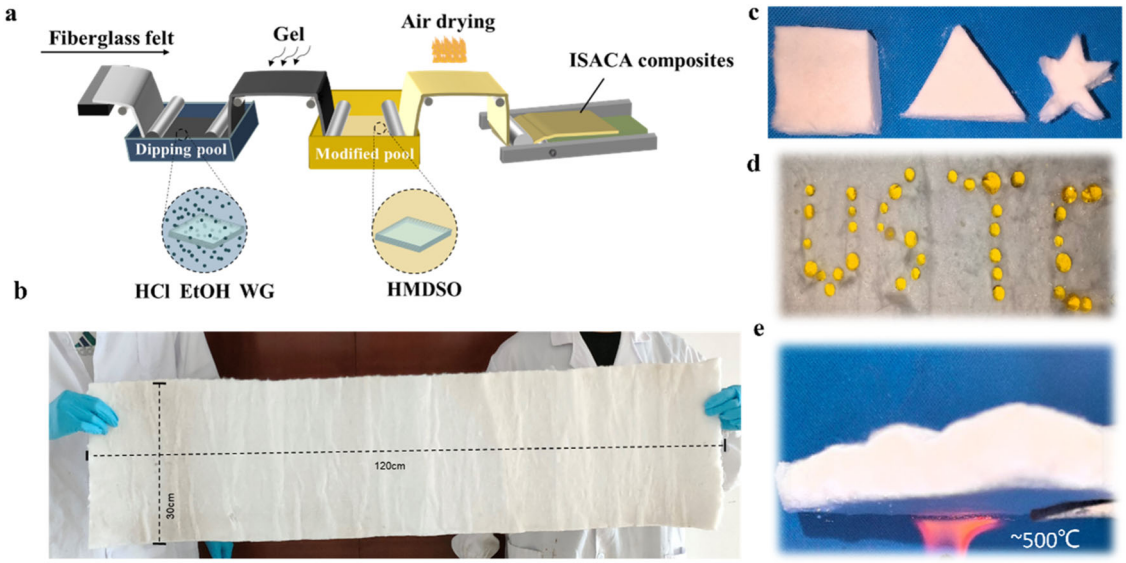

Fig. 1 **a** Schematic illustration of the fabrication of ISACA. **b** A large sample of the ISACA composites. **c** Photograph of ISACA composites with various shapes. **d** The stained water beads on ISACA composites proved their good hydrophobicity. **e** ISACA composites exhibit excellent high temperature resistance when exposed to the flame of an alcohol lamp

the beaker, which was then heated and stirred in a water bath at 65 °C for 2 h. Finally, the modified powder was placed in a drying oven at 120 °C for 1 h to obtain ISACA powder.

2.3 Preparation of ISACA composites

The procedure of fabrication of ISACA composites is schematically presented in Fig. 1a. Firstly, the glass fiber felt was immersed in the prepared sol, which was configured according to the dilution of water glass (0.88 mol/L): hydrochloric acid (HCl, 11.9 mol/L): ethanol: water = 2.5:2.5:1.5:1. The gelation usually occurred in 3 min. After aging at 75 °C for 1 h, the wet gel composite is immersed in hydrophobization agent for hydrophobic modification at 75 °C for 4 h. Finally, under ambient pressure drying at 200 °C for 1 h, ISACA composites can be obtained.

2.4 Characterization

The pore size distribution was measured using a fully automated specific surface area and porosity analyzer (TriStar II 3020M). The microstructure of the samples was characterized by scanning electron microscopy (SEM, SU8220). XPS (ESCALAB 250Xi) were conducted to analyze the elemental composition. XRD (TTR-III) analysis was used to analyze the phases. The densities of aerogels were assessed based on the standard of ISO 845:2006. The Brunauer–Emmett–Teller (BET) method obtained the specific surface area. The pore size distribution was determined using the Barret-Joyner-Halenda (BJH) method and the desorption branch of the isotherms. A Fourier transforms infrared (FTIR) spectra was obtained on KBr pellets with a Nicolet iN10 infrared spectrometer (Supplementary Fig. S2).

Mechanical properties were studied by using the universal testing machine (Instron E3000K8953) and dynamic thermomechanical analyzer (DMA, TA Q800). The thermal conductivity of sample was measured employing the Hot Disk technique (TPS2500S). Thermogravimetry-differential scanning calorimetry (TG-DSC) (SDT Q600) was performed to analyze the pyrolysis process. The thermal insulation property was characterized by the infrared thermal imager (FLIR A655sc).

3 Results and discussion

3.1 Fabrication

The ISAC strategy can be utilized for the preparation of a larger-scale ISACA sample ($120 \times 30\ cm^2$), as illustrated in Fig. 1b, showcasing the method's scalability. Besides, the ISACA composites exhibit high machinability and can be customized into various shapes to meet the complex geometric requirements of practical applications (Fig. 1c). Also, we drop stained water onto the composite, and the water forms droplets on the surface. This phenomenon indicates the extraordinary hydrophobic properties of the composite (Fig. 1d, Supplementary Fig. S1). After being burned by the outer flame of the alcohol lamp, the structure remains intact, which proves that it has excellent high temperature resistance (Fig. 1e).

The ISAC strategy significantly reduces raw materials and processing time. The entire production cycle takes

only 6 h, including gel, aging, hydrophobic modification and APD. The solvent exchange step has been removed, which is important to the traditional preparation process. The acidic catalyst used in the gelation and the modification has been added to the sol in advance. The hydrogen ion concentration in the sol can be controlled by adjusting the addition amount of hydrochloric acid. The addition amount of each component and the gel time under different hydrogen ion concentrations are shown in Table 1. The progressive acidification process of sodium monosilicate ions in a strong acid solution is shown in Fig. 2a. In a higher acid concentration, the process of sol gelling is shown in Fig. 2b.

The pore size distribution (PSD) of silica aerogel powder S1–S5 is displayed in Fig. 3a. The produced aerogels' PSD had a distinct unimodal distribution. A more homogeneous PSD and a smaller pore size were the outcomes of raising the $[H^+]$. A wide PSD with a peak value of about 15 nm was seen when the $[H^+] = 2.0$ mol/L (S1). This indicates that the PSD is inhomogeneous. There was a narrow peak about 8 nm as the $[H^+]$ increased to 4.0 mol/L (S5). This indicates that when $[H^+] = 4$ mol/L, the pore size in the sample is uniformly distributed around 8 nm. As shown in Fig. 3b, as the concentration of hydrogen ions in the sol continues to increase, the density of the powder continues to decrease and the specific surface area continues to increase. The porosity of the samples is shown in Supplementary Table S1. Figure 3c shows the XRD patterns of the ISACA. The broad diffraction peaks were observed at $2\theta = 22°$. A low crystallinity degree is indicated by the characteristic peaks of the SiO_2 aerogels with alkyl groups. Figure 3d illustrated SiO_2 aerogels' formation in the ISAC by X-ray photoelectron spectroscopy (XPS) results. When $[H^+] = 4.0$ mol/L, the aerogel has the best performance. When the $[H^+]$ exceeds 4.0 mol/L, stable gel cannot be formed, which is not suitable for this study. Therefore, the maximum $[H^+]$ of this work is 4.0 mol/L.

The microstructure of the aerogels (Fig. 4) can also reflect the condition mentioned above. It can be seen that when the $[H^+] = 2.5$ mol/L, there are fewer pores between aerogels, and no clear skeleton structure can be observed. When the $[H^+]$ increases, it can be intuitively observed that the pores in the aerogel structure continue to increase, the aerogel skeleton becomes more and more obvious, and even a "fibrous" skeleton structure appears. When the $[H^+]$ in the sol reaches 4.0 mol/L, the aerogel structure is the most stable.

Table 1 The content of each component in the sol of different samples

Sample	1	2	3	4	5
$[H^+]$ in sol (mol/L)	2.0	2.5	3.0	3.5	4.0
HCl (ml)	58	72	87	101	116
Water (ml)	82	68	53	39	24
Gelling time (min)	130	50	23	10	3

All samples: Water glass 100 ml, EtOH 60 ml

3.2 In-situ acid catalysis strategy

The conventional steps for preparation of aerogel composites are: gel, aging, displacement, modification, and drying. However, the ISAC strategy has the advantage of eliminating the displacement step, which is extremely time

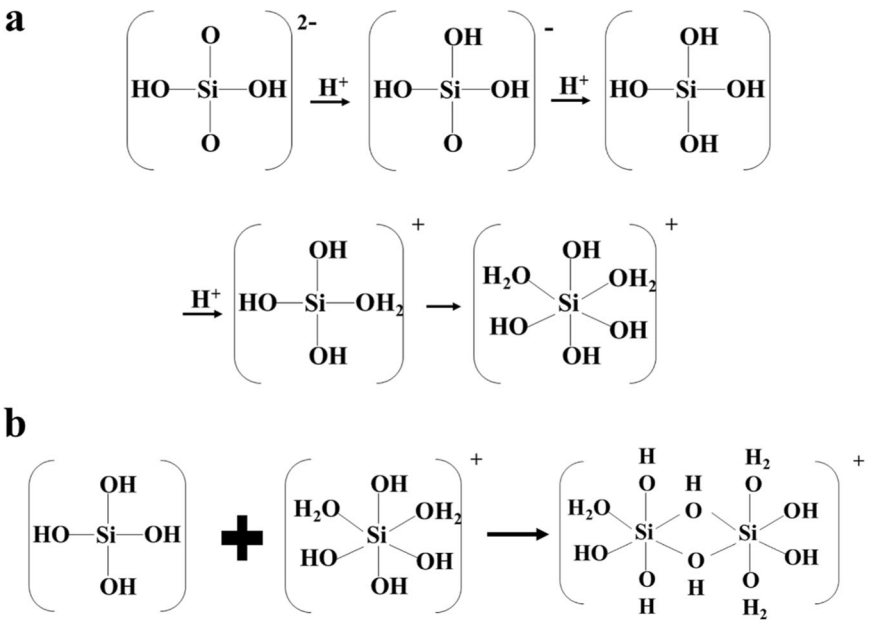

Fig. 2 **a** The progressive acidification process of sodium monosilicate ions in a strong acid solution. **b** The sol–gel process in higher acid concentrations

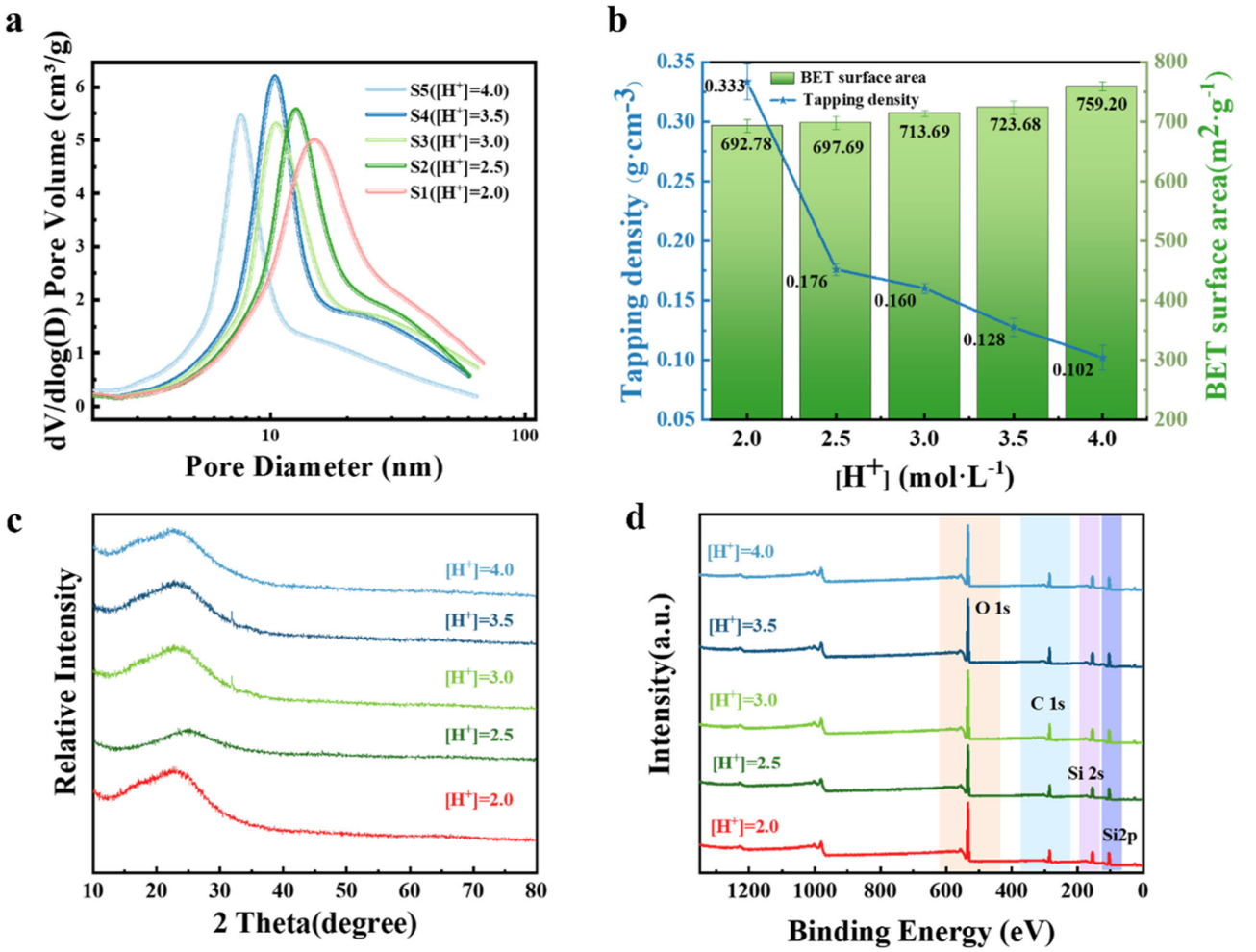

Fig. 3 **a** The PSD, **b** the vibrational density and specific surface area, **c** XRD pattern and **d** XPS of the samples prepared with different [H^+]

consuming, and thus greatly shorting the preparation cycle. In the case of non-in-situ catalytic modification—according to the conventional preparation steps, if the replacement process is also omitted and the acidic catalyst is directly added to the modified solution, the aerogels cannot be completely modified, and only a small part can be successfully modified (Fig. 5a). In order to have a more intuitive comparison, methyl orange indicator was added to the sol solution. At 25 °C, methyl orange appears red in a medium with the pH less than 3.1, yellow in a medium with the pH greater than 4.4, and orange when the pH is between 3.1 and 4.4. HMDSO is cheaper than chlorotrimethylsilane (TMCS) and does not produce HCl as a by-product, but it needs to add acid to catalyze the alkane silication process during modification. And HMDSO is an oily substance that is not compatible with water. Therefore, in the case of off-situ acid catalytic modification, the acid catalyst is directly added to the modification solution without the replacement step, and the solution delamination occurs. The upper layer is the modifier, and the lower layer is the aqueous phase, including acid and most of ethanol. This results in the off-situ acid catalytic modification, only the place where the two phases are in contact is partially modified, and the other places are modified. In the in-situ acid catalytic modification strategy, because the acid catalyst is included in the sol prior to gelation, it is homogeneously dispersed through the mesopores of the gel, resulting in much reduced hydrophobization time. The thermal conductivity of the aerogel composite prepared by this method is 0.01499 $W \cdot m^{-1} K^{-1}$ at room temperature, while the conventional method is 0.0234 $W \cdot m^{-1} K^{-1}$ [23].

The surface of silica hydrogels undergoes a transformation to nonpolarity following the grafting of alkyl or aryl groups throughout the surface modification process. This alteration effectively prevents the condensation reaction between the Si-OH groups within the pores of the silica hydrogels [24]. In this study, silica hydrogels underwent modification through the substitution of -OH groups with -Si $(CH_3)_3$. The hydrolytically stable -Si $(CH_3)_3$ groups present in HMDSO are capable of replacing Si-OH groups

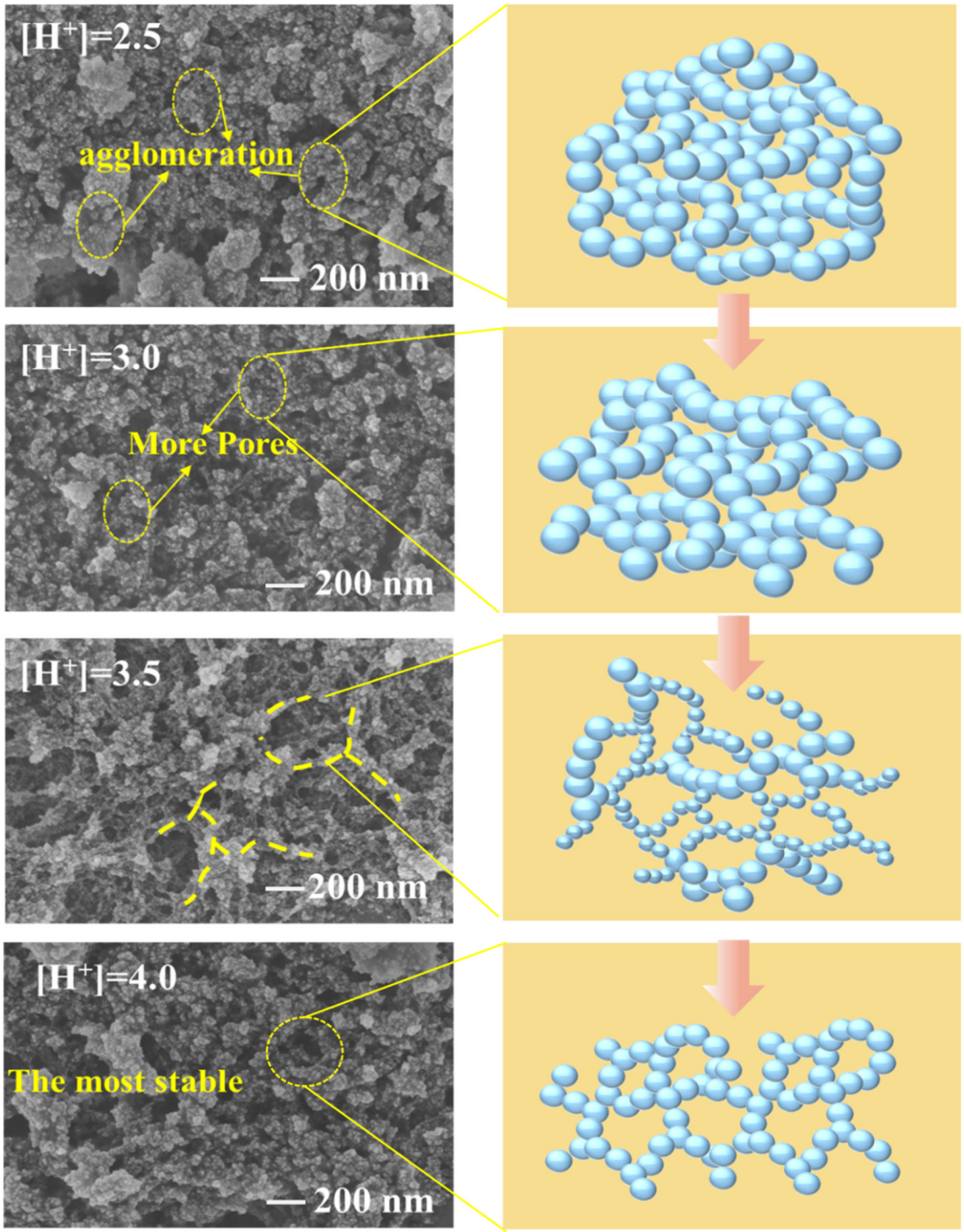

Fig. 4 SEM images and structure diagrams of aerogel powders prepared by different $[H^+]$

on the surface of silicon oxide (Fig. 5b). The inset of Supplementary Fig. S1 displays a photograph of water droplets on the surface of SiO_2 aerogel composites. The aerogels' superhydrophobic properties further demonstrate the successful hydrophobization of the silica hydrogels via the ISAC method.

3.3 Mechanical properties

In practical production applications, SiO_2 aerogel composites must be capable of withstanding long-term and high-frequency mechanical shocks. To investigate the elasticity and fatigue resistance of ISACA composites, experiments

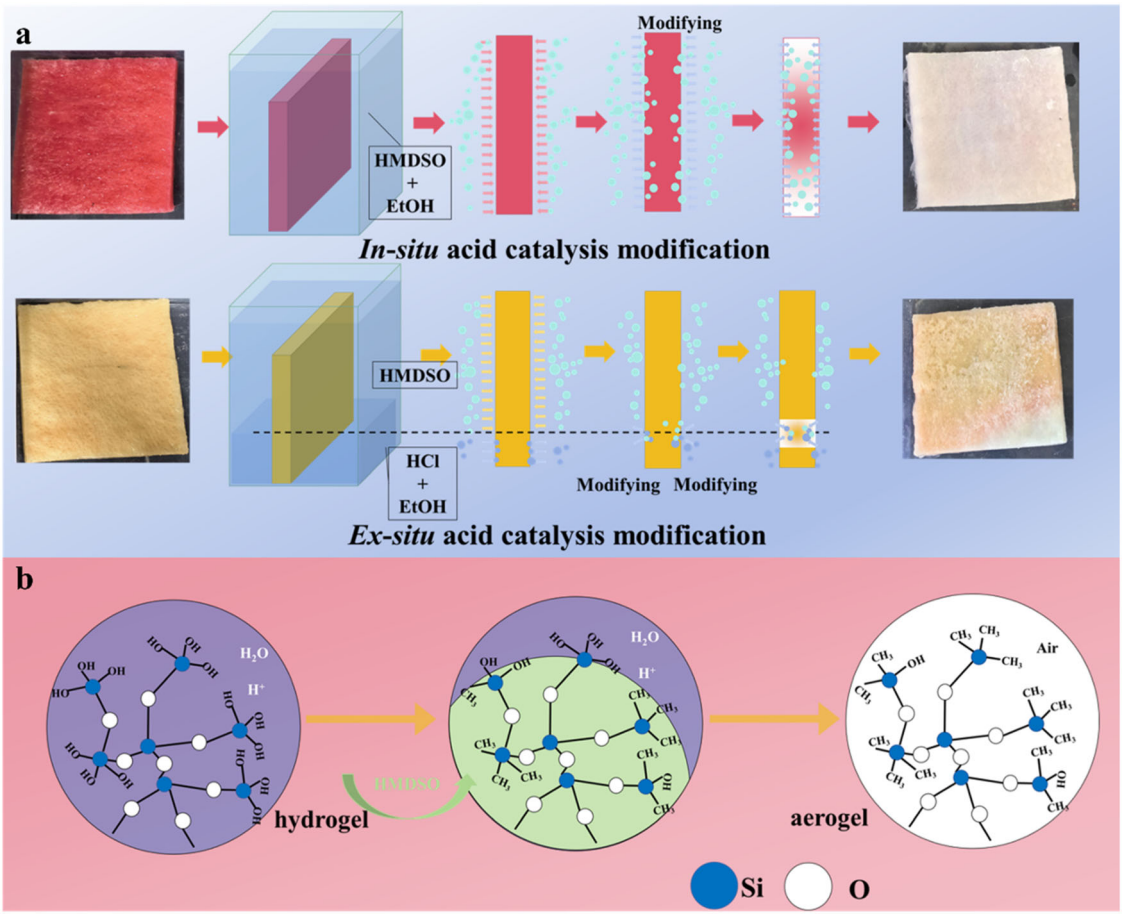

Fig. 5 **a** Comparison of in-situ acid-catalyzed modification with non-in-situ acid-catalyzed modification. **b** Modification mechanism diagram

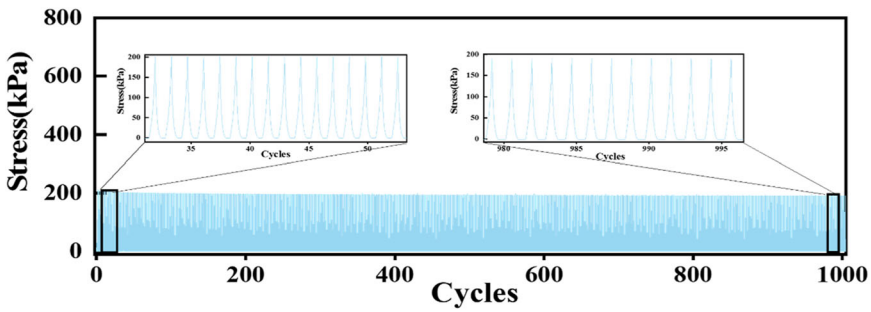

Fig. 6 Stress–cycles curves of the ISACA composites in 1000 loading–unloading fatigue cycles

were conducted using a universal testing machine. A sequence of tests involving 1000 loading–unloading cycles was performed to assess the fatigue resistance of the ISACA composites at a maximum strain (ε) of 40%, with a loading rate of 60 mm/min. The ISACA composites demonstrated the ability to endure up to 40% elastic deformation (ε) (Fig. 6).

Compression tests along the layer-stacking direction at various ε values of 15, 30, and 40% showed that ISACA composites possess considerable mechanical robustness. The compression stress was recorded at 100 kPa for 30% strain, increasing to 200 kPa at a compression strain of 40% (Fig. 7a). ISACA composites exhibited outstanding cyclic durability in loading–unloading fatigue test at 40% strain (Fig. 7b), with only a 3% deformation observed after 1000 cycles. Young's modulus was measured following 1000 compression cycles (Fig. 7c). After undergoing 1000 cycles, ISACA composites maintained a low energy loss coefficient of nearly 0.04 from the 10th cycle, preserving over 90% of maximum stress. The Young's modulus of the composite exhibited a slight increase before stabilizing. The low

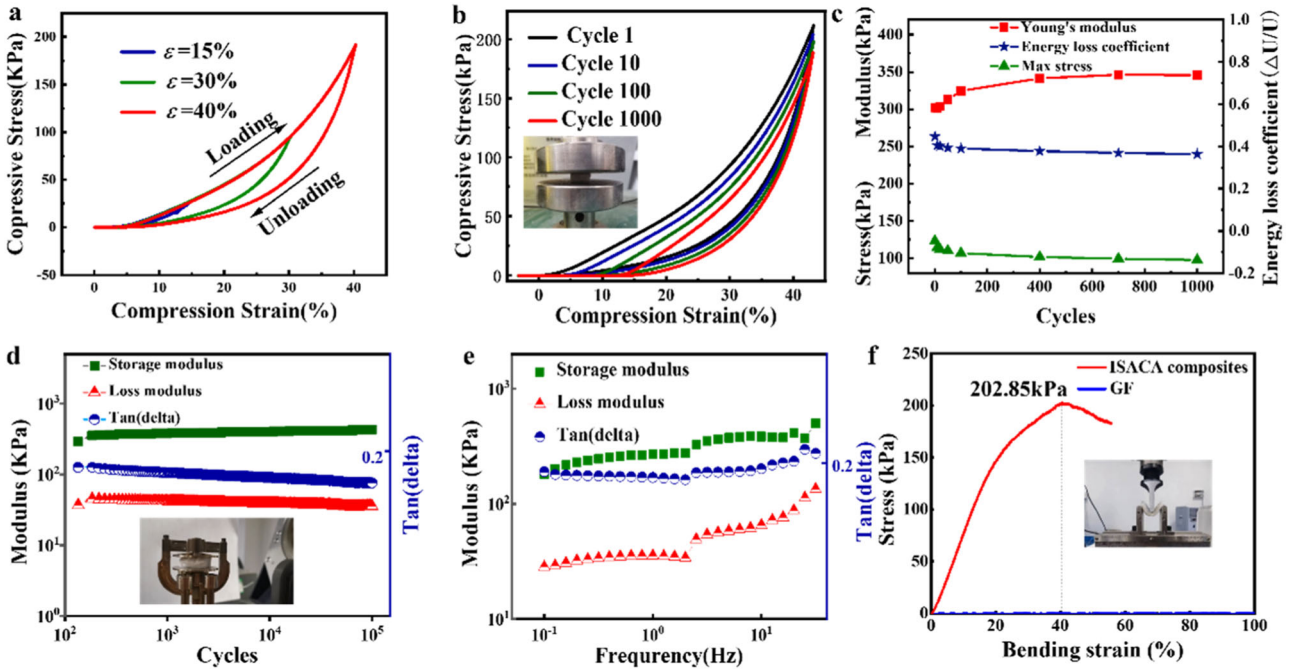

Fig. 7 Mechanical properties of the ISACA composites. **a** Compressive σ versus ε curves during loading–unloading cycles at different ε amplitude. **b** 1000 cyclic fatigue test (compression $\varepsilon = 40\%$). **c** Young's modulus, maximum stress, and energy loss coefficient as a function of compressive cycles. **d** Storage modulus, loss modulus, and damping ration of the ISACA composites in the 100,000 cycles of the DMA test. **e** The frequency dependence of the storage modulus, loss modulus, and damping ratio for ISACA composites (oscillatory ε of 3%). **f** The three-point bending test of ISACA composites

energy loss coefficient signifies minimal energy dissipation throughout the loading–unloading cycles, while the silica aerogel's three-dimensional structure contributes to the composite's high compression resistance.

Dynamic mechanical analysis (DMA) test was conducted to evaluate the mechanical robustness and fatigue resistance of ISACA composites under 1% oscillatory strain across 100,000 cycles, further investigating their fatigue resistance. Remarkably, the outcomes of these tests on ISACA composites were unexpected (Fig. 7d). The storage and loss moduli of the ISACA composites were comparable to those of the previously reported super-elastic aerogels [25–27], indicating outstanding fatigue resistance. Meanwhile, dynamic compression test, conducted at an oscillatory strain (ε) of 1%, revealed a nearly constant storage modulus, loss modulus, and damping ratio across a frequency range of 0.1–30 rad/s, further highlighting the robust mechanical properties of ISACA composites (Fig. 7e). The maximum bending modulus of glass fiber (GF) registers at 7.25 kPa. When integrated with the ISAC strategy and SiO_2 aerogels, the composite material exhibits a maximum bending modulus of 202.85 kPa, representing an approximate 28-fold increase. This enhancement has been validated through three-point bending and uniaxial compression tests (Fig. 7f). The ISACA composites exhibit significantly enhanced impact resistance and mechanical robustness

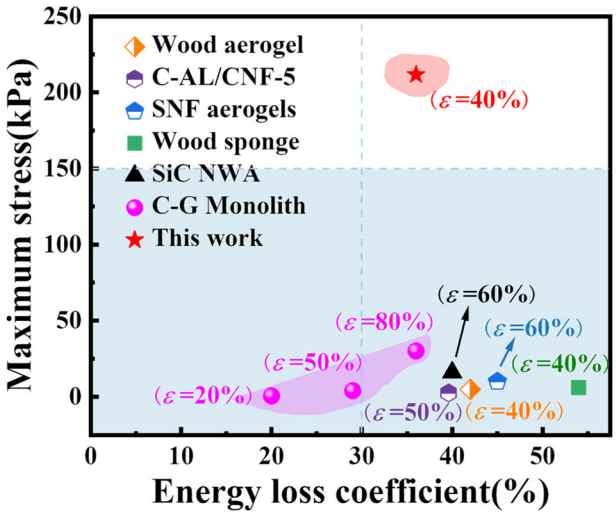

Fig. 8 A comparison of properties between ISACA composites with other similar elastomeric materials previously reported

compared to similar elastomeric materials documented in previous reports (Fig. 8) [28–33].

3.4 Thermal insulation properties

An infrared thermal imager was utilized to capture the temperature distribution and its changes over time in order to more precisely describe the ISACA composites' thermal

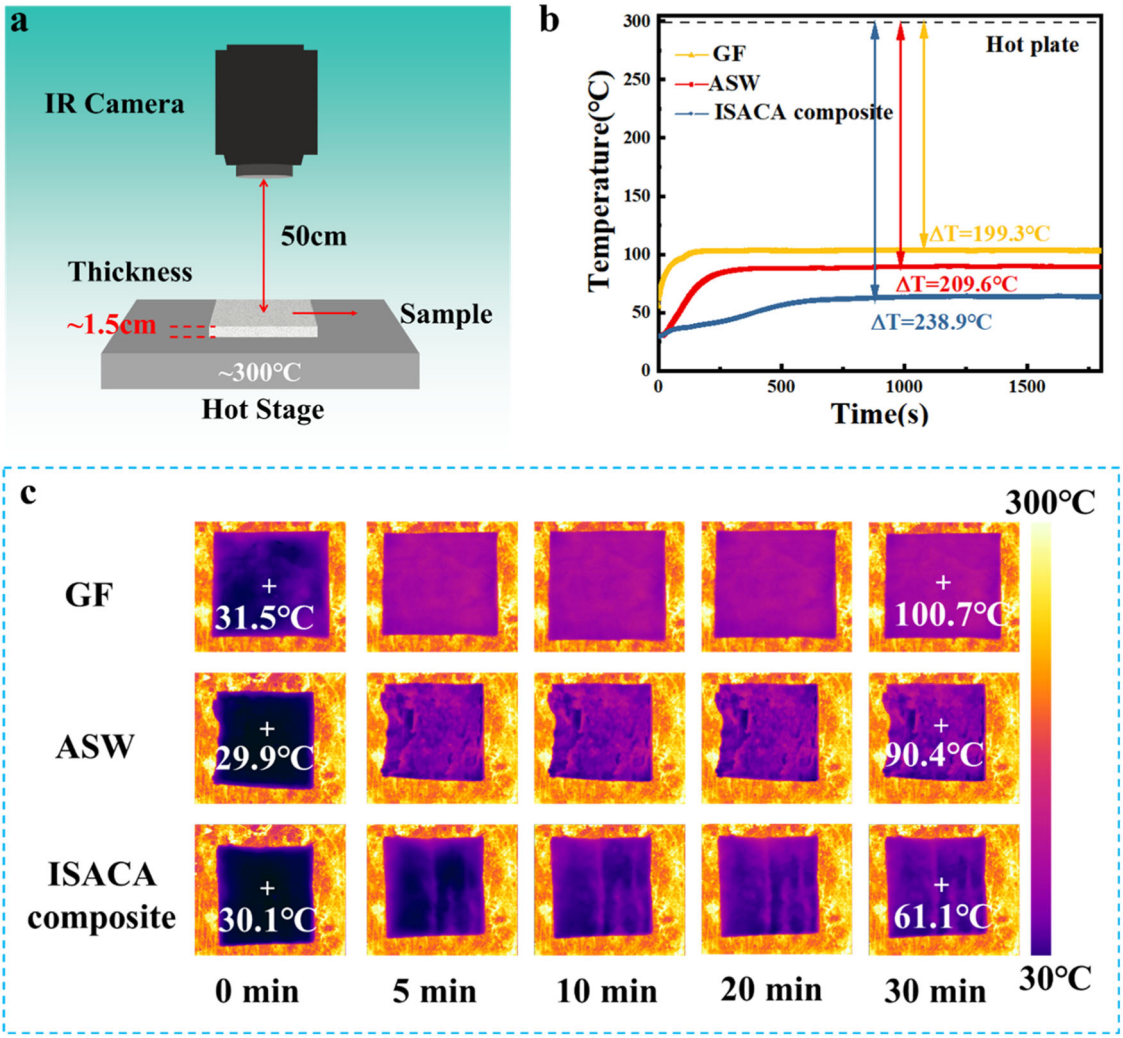

Fig. 9 **a** Diagram showing the use of a thermal infrared imager to observe a sample that has been heated by a hot plate. **b** The temperature curves for the appropriate time-surface in **c**. **c** Infrared contrast image of hot-plate heated glass fiber (GF), aluminum silicate cotton (ASW) and ISACA composite samples

insulation capabilities. First, a 300 °C hot plate simulated a moderately high-temperature operating environment. Different types of samples (GF, ASW, and ISACA composites) were placed on the hot plate (Fig. 9a). The infrared thermal imager continuously recorded the upper surface temperature of the samples (Fig. 9c). As illustrated in Fig. 9b, upon heating, the sample surface temperature increased gradually before stabilizing. After 30 min of heating, the upper surface temperature of GF reached 100.7 °C, while that of ASW was 90.4 °C. In comparison, the upper surface temperature of the ISACA composite was 61.1 °C. These results indicate that ISACA composites adequately fulfill the thermal insulation requirements for these temperature scenarios.

In addition, we built ourselves a device to test the thermal insulation properties of the material. The device is heated by a Muffle furnace, which simulates the actual application of the sample in everyday life. Infrared thermograph, thermocouple and module are used to monitor the surface temperature change of the test sample, and computer is used to record and process the data (Fig. 10a). Measurements of the heat insulation and fire resistance of GF, ASW, and ISACA composite (1 cm thickness) are shown in an optical picture (Fig. 10c). Using an infrared camera and thermocouple temperature collector, the sample's qualitative thermal insulation on the self-built platform is captured, displaying a gradient temperature distribution on the back of ISACA composites (Fig. 10c). At first, the back-side surface's temperature increased gradually. The samples' backside surface temperature became smooth and steady after 30 min of exposure to the heat radiation from the Muffle Furnace, reaching a maximum temperature of roughly 101.3 °C (GF), 98.4 °C (ASW), and 88.6 °C (ISACA composite) (Fig. 10b). The temperature difference

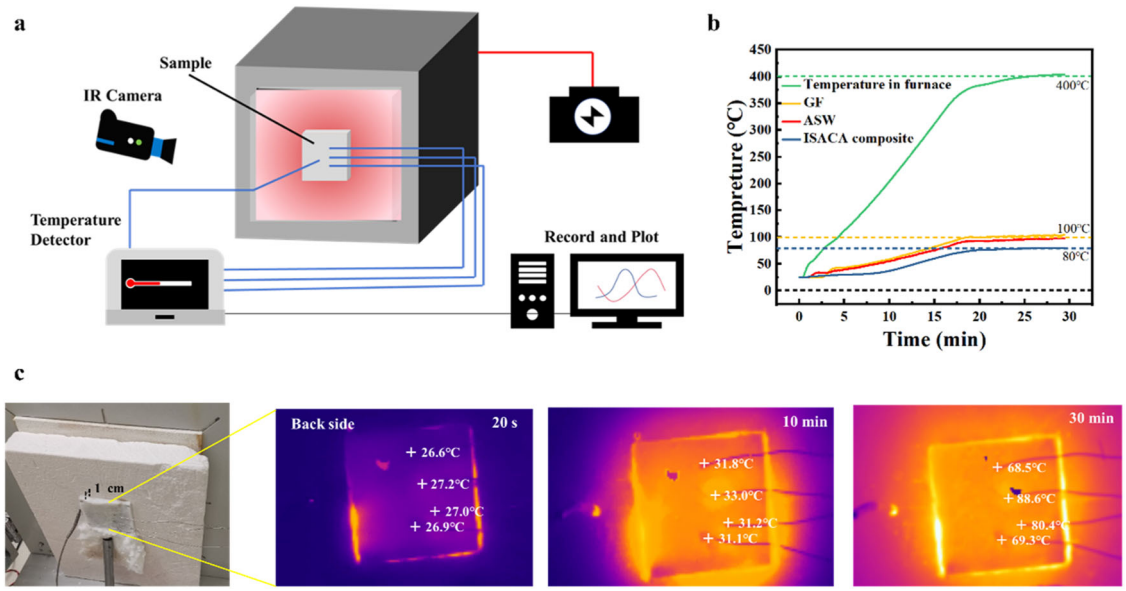

Fig. 10 **a** Self-built sample thermal insulation performance test platform diagram. **b** Time-temperature function diagram of thermocouples at each part of the test platform. **c** Optical and Infrared images of the back side during the 30 min heating process of self-built sample thermal insulation test platform

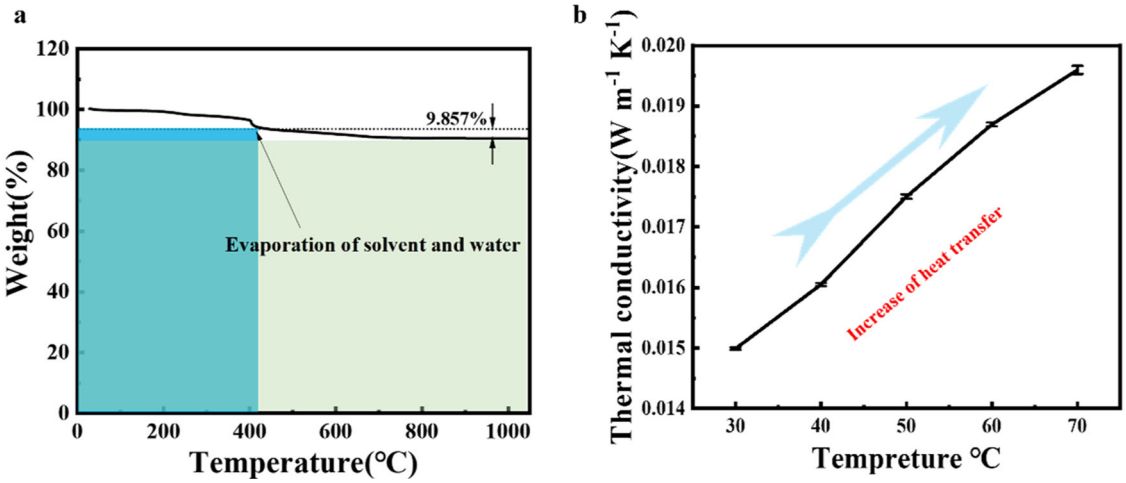

Fig. 11 **a** TG curve of ISACA composites. **b** The ISACA composites' thermal conductivities at various temperatures

was maintained at 300 °C in comparison to a high heating source of 400 °C, demonstrating the enormous potential of ISACA composite in high temperature applications [34].

As seen in Fig. 11a, thermogravimetric analysis (TGA) was used to examine the ISACA composites' tolerance to high temperatures. Upon reaching approximately 423 °C, a reduction in mass was observed, suggestive of a small number of organic molecules and physically adsorbed water evaporating, contributing to 5.99% of the total mass of ISACA composite. A further mass loss, constituting 3.79% of the overall mass, was noted. This additional decrease in mass is associated with the process of hydroxyl group condensation, leading to dehydration and the formation of Si-O-Si bonds [35], thereby enhancing the SiO_2 network, as demonstrated by the reaction:

$$\equiv Si - OH + HO - Si \equiv \rightarrow \equiv Si - O - Si \equiv + H_2O$$

Additionally, at various temperatures, we examined the ISACA composites' thermal conductivity variation law (Fig. 11b). The findings demonstrated that thermal conductivity progressively rose as temperature rose, mostly as a result of an increase in thermal radiation at high temperatures.

Heat conduction through fibers and aerogel, heat transfer through air, and thermal radiation are all included in the heat transfer mode for ISACA composites. (Fig. 12a) [36]. Heat transmitted through (1) aerogel Q_{ae}, (2) aerogel and fibers Q_{ae+f}, (3) air Q_{air}, and (4) radiation heat through

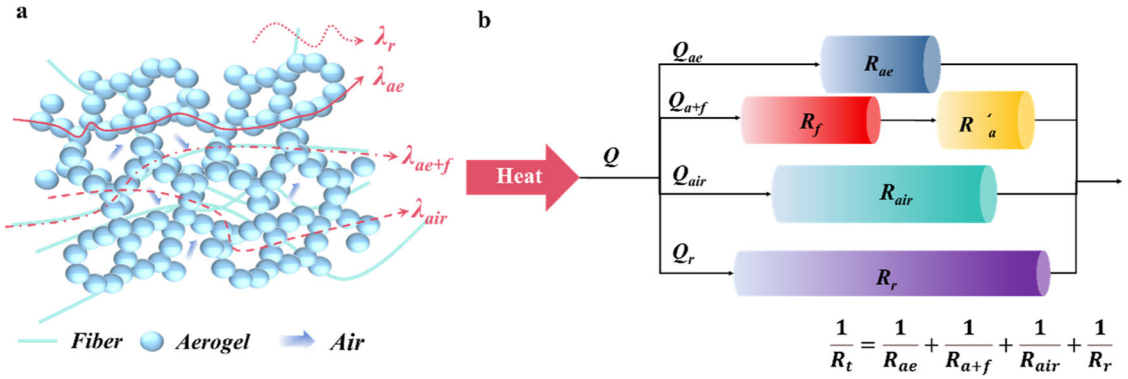

Fig. 12 **a** An illustration of heat transfer. **b** The parallel thermal resistance of the fibers, aerogel, air, and radiation

former pathways Q_r make up the total heat flux. The parallel thermal resistance of the appropriate part equals the total equivalent thermal resistance of the ISACA composites (Fig. 12b). The formula for total thermal resistance (Eq. (1)) can be obtained using the Fourier equation $Q = \Delta T/R = \lambda_t S_t/l_t \Delta T$.

$$1/R_t = 1/R_{ae} + 1/R_{ae+f} + 1/R_{air} + 1/R_r \quad (1)$$

The heat radiation can be compared to the radiation between two virtual planes of incoming and outgoing with temperatures T_1 and T_2, since it is assumed that there is a one-dimensional steady-state heat transfer. The radiant heat flux can be stated as follows in the radiant heat transfer energy balance equation:

$$Q_r = \lambda_r S_r/l_r \Delta T = S_r G\varepsilon\sigma\left(T_1^4 - T_2^4\right) = 4S_r G\varepsilon\sigma T_m^3 \Delta T \quad (2)$$

When $l_r = L_0$, the thermal resistance to radiation is provided,

$$\lambda_r = 4L_0 G\varepsilon\sigma T_m^3 = FL_0 T_m^3 \quad (3)$$

Consequently, the ISACA composites' room temperature thermal conductivity formula (Eq. (4)).

$$\lambda_r = \left(1 - \nu^{1/2}\right)\lambda_{ae} + x(\lambda_{air} - \lambda_{ae}) + Fa/\nu^{1/2} T_m^3 \quad (4)$$

where ν and x represent the relative volume fractions of air and fiber in ISACA composites. The air section's thermal conductivity is represented by λ_{air}, while SiO_2's thermal conductivity is represented by λ_{ae}. The thermal radiation synthesis constant is given by $F = 4G\varepsilon\sigma$, where G is the radiation shape factor and has a range of 0 to 1. The average temperature of the unit cube is T_m, and it may be found by

$$T_m^3 = T_1^3 + T_1^2 T_2 + T_1 T_2^2 + T_2^3/4$$

4 Conclusion

In summary, we report a new strategy for the ultra-rapid synthesis of silica aerogels featuring exceptional thermal insulation, high porosity, and extensive specific surface area, achieved through in situ acid catalysis. The synthesized ISACA composites exhibit remarkable elasticity, boasting a bending resistance up to 30 times greater than previously observed. Furthermore, these composites demonstrate outstanding thermal insulation, characterized by an ultra-low thermal conductivity of merely 0.01499 $W \cdot m^{-1} K^{-1}$ at ambient temperature. Crucially, the mechanism behind gel modification through the in-situ acid catalysis method is clarified by contrasting it with gel modifications in HMDSO. Because the acid catalyst is included in the sol prior to gelation, it is homogeneously dispersed through the mesopores of the gel, resulting in much reduced hydrophobization time. Additionally, we are able to modify the pore structure of silica aerogels by varying the concentration of hydrogen ions during gelation. We contend that this study offers novel insights into the cost-effective and expedited synthesis of silica aerogels.

Supplementary information The online version contains supplementary material available at https://doi.org/10.1007/s10971-024-06518-2.

Acknowledgements This work was financially supported by Collaborative Innovation Program of Universities in Anhui Province (GXXT-2022-018), National Natural Science Foundation of China (No.52374238, 52104226 and U2233202), Youth Innovation Promotion Association (No.CX2320007001), Key Laboratory of Fire Protection Technology for Industry and Public Building, Ministry of Emergency Management (No. 2022KLIB02).

Author contributions Zun Zhao conducted the experiment and wrote the main manuscript text. Yuelei Pan and Xudong Cheng devised the project, the main conceptual ideas and proof outline. Mingyuan Yan guided the writing of the entire manuscript text. Yueyue xiao prepared figure12 and performed the analytic calculations. Hui Yang and Xudong Cheng were involved in planning and supervised the work. All authors reviewed the manuscript.

Compliance with ethical standards

Conflict of interest The authors declare no competing interests.

References

1. Yan M, Cheng X, Shi L, Pan Y, He P, Zhang Z, Lun Z, Fu Y, Zhang H (2023) Bioinspired SiC aerogels for super thermal insulation and adsorption with super-elasticity over 100,000 times compressions. Chem Eng J 455:140616. https://doi.org/10.1016/j.cej.2022.140616
2. Yan M, Cheng X, Gong L, Lun Z, He P, Shi L, Liu C, Pan Y (2023) Flexible SiC nanowire/mullite fiber composite aerogel with adjustable strength based on micromechanical design. Chem Eng J 466:143089. https://doi.org/10.1016/j.cej.2023.143089
3. Yan MY, Cheng XD, Gong LL, Lun ZY, He P, Shi L, Liu CJ, Pan YL (2023) Growth mechanism and structure regulation of super-elastic SiC aerogels for thermal insulation and electromagnetic wave absorption. Chem Eng J 475, https://doi.org/10.1016/j.cej.2023.146417
4. Gurav JL, Jung I-K, Park H-H, Kang ES, Nadargi DY (2010) Silica Aerogel: Synthesis and Applications. J Nanomater 2010:1–11. https://doi.org/10.1155/2010/409310
5. Li C, Chen Z, Dong W, Lin L, Zhu X, Liu Q, Zhang Y, Zhai N, Zhou Z, Wang Y, Chen B, Ji Y, Chen X, Xu X, Yang Y, Zhang H (2021) A review of silicon-based aerogel thermal insulation materials: Performance optimization through composition and microstructure. J Non Crystalline Solids 553:120517. https://doi.org/10.1016/j.jnoncrysol.2020.120517
6. Pan Y, He S, Cheng X, Li Z, Li C, Huang Y, Gong L (2017) A fast synthesis of silica aerogel powders-based on water glass via ambient drying. J Sol Gel Sci Technol 82(2):594–601. https://doi.org/10.1007/s10971-017-4312-4
7. Pan Y, Cheng X, Zhou T, Gong L, Zhang H (2018) Spray freeze-dried monolithic silica aerogel based on water-glass with thermal superinsulating properties. Mater Lett 229:265–268. https://doi.org/10.1016/j.matlet.2018.07.035
8. Cheng X, Zhu S, Pan Y, Deng Y, Shi L, Gong L (2020) Fire retardancy and thermal behaviors of Cellulose nanofiber/zinc borate aerogel. Cellulose 27(13):7463–7474. https://doi.org/10.1007/s10570-020-03289-1
9. Yoldas BE, Annen MJ, Bostaph J (2000) Chemical engineering of aerogel morphology formed under nonsupercritical conditions for thermal insulation. Chem Mater 12(8):2475–2484. https://doi.org/10.1021/cm9903428
10. Henning S, Svensson L (1981) Production of silica aerogel. Phys Scr 23(4):697–702. https://doi.org/10.1088/0031-8949/23/4b/018
11. Dorcheh AS, Abbasi MH (2008) Silica aerogel; synthesis, properties and characterization. J Mater Process Technol 199(1-3):10–26. https://doi.org/10.1016/j.jmatprotec.2007.10.060
12. Shrinivasan S, Norris PM (2005) Aerogels: unique material, fascinating properties and unlimited applications. Annu Rev Heat Transf 14:385–408
13. Haqa EU, Syed FAZ, Muhammad Z, Muhammad RAK, Sanosh KP, Licciulli A (2017) Hydrophobic silica aerogel glass-fibre composite with higher strength and thermal insulation based on MTMS precursor. Energy Build 151:494–500. https://doi.org/10.1016/j.enbuild.2017.07.003
14. Zhang X, Li W, Song P, You B, Sun G (2020) Double-cross-linking strategy for preparing flexible, robust, and multifunctional polyimide aerogel. Chem Eng J 381:122784. https://doi.org/10.1016/j.cej.2019.122784
15. He S, Huang D, Bi H, Li Z, Yang H, Cheng X (2015) Synthesis and characterization of silica aerogels dried under ambient pressure bed on water glass. J Non Crystalline Solids 410:58–64. https://doi.org/10.1016/j.jnoncrysol.2014.12.011
16. Bhagat SD, Kim Y-H, Moon M-J, Ahn Y-S, Yeo J-G (2007) A cost-effective and fast synthesis of nanoporous SiO2 aerogel powders using water-glass via ambient pressure drying route. Solid State Sci 9(7):628–635. https://doi.org/10.1016/j.solidstatesciences.2007.04.020
17. Li Z, Gong L, Cheng X, He S, Li C, Zhang H (2016) Flexible silica aerogel composites strengthened with aramid fibers and their thermal behavior. Mater Des 99:349–355. https://doi.org/10.1016/j.matdes.2016.03.063
18. Li Z, Cheng X, He S, Shi X, Gong L, Zhang H (2016) Aramid fibers reinforced silica aerogel composites with low thermal conductivity and improved mechanical performance. Compos Part A Appl Sci Manuf 84:316–325. https://doi.org/10.1016/j.compositesa.2016.02.014
19. Yu H, Jiang Y, Lu Y, Li X, Zhao H, Ji Y, Wang M (2019) Quartz fiber reinforced Al2O3-SiO2 aerogel composite with highly thermal stability by ambient pressure drying. J Non Crystalline Solids 505:79–86. https://doi.org/10.1016/j.jnoncrysol.2018.10.039
20. Wu H, Liao Y, Ding Y, Wang H, Peng C, Yin S (2014) Engineering Thermal and Mechanical Properties of Multilayer Aligned Fiber-Reinforced Aerogel Composites. Heat Transf Eng 35(11-12):1061–1070. https://doi.org/10.1080/01457632.2013.863090
21. Yi Z, Zhang X, Yan L, Huyan X, Zhang T, Liu S, Guo A, Liu J, Hou F (2022) Super-insulated, flexible, and high resilient mullite fiber reinforced silica aerogel composites by interfacial modification with nanoscale mullite whisker. Compos Part B Eng 230:109549. https://doi.org/10.1016/j.compositesb.2021.109549
22. Yi Z, Yan L, Zhang T, Guo A, Liu J, Jin W, Liu S, Jing W, Hou F (2020) Thermal insulated and mechanical enhanced silica aerogel nanocomposite with in-situ growth of mullite whisker on the surface of aluminum silicate fiber. Compos Part A Appl Sci Manuf 136:105968. https://doi.org/10.1016/j.compositesa.2020.105968
23. Liu Z, Zang C, Zhang S, Zhang Y, Yuan Z, Li H, Jiang J (2021) Atmospheric drying preparation and microstructure characterization of fly ash aerogel thermal insulation material with super-hydrophobic. Constr Build Mater 303:124425. https://doi.org/10.1016/j.conbuildmat.2021.124425
24. Kim Y-G, Kim HS, Jo SM, Kim SY, Yang BJ, Cho J, Lee S, Cha JE (2018) Thermally insulating, fire-retardant, smokeless and flexible polyvinylidene fluoride nanofibers filled with silica aerogels. Chem Eng J 351:473–481. https://doi.org/10.1016/j.cej.2018.06.102
25. Jia C, Li L, Liu Y, Fang B, Ding H, Song J, Liu Y, Xiang K, Lin S, Li Z, Si W, Li B, Sheng X, Wang D, Wei X, Wu H (2020) Highly compressible and anisotropic lamellar ceramic sponges with superior thermal insulation and acoustic absorption performances. Nat Commun 11(1):3732. https://doi.org/10.1038/s41467-020-17533-6
26. Dou L, Zhang X, Shan H, Cheng X, Si Y, Yu J, Ding B (2020) Interweaved Cellular Structured Ceramic Nanofibrous Aerogels with Superior Bendability and Compressibility. Adv Functional Mater 30 (49). https://doi.org/10.1002/adfm.202005928
27. Zong D, Cao L, Yin X, Si Y, Zhang S, Yu J, Ding B (2021) Flexible ceramic nanofibrous sponges with hierarchically entangled graphene networks enable noise absorption. Nat Commun 12(1):6599. https://doi.org/10.1038/s41467-021-26890-9
28. Song J, Chen C, Yang Z, Kuang Y, Li T, Li Y, Huang H, Kierzewski I, Liu B, He S, Gao T, Yuruker SU, Gong A, Yang B, Hu L (2017) Highly Compressible, Anisotropic Aerogel with Aligned

Cellulose Nanofibers. ACS Nano 12(1):140–147. https://doi.org/10.1021/acsnano.7b04246
29. Chen Z, Zhuo H, Hu Y, Lai H, Liu L, Zhong L, Peng X (2020) Wood-Derived Lightweight and Elastic Carbon Aerogel for Pressure Sensing and Energy Storage. Adv Functional Mater 30 (17). https://doi.org/10.1002/adfm.201910292
30. Wang F, Dou L, Dai J, Li Y, Huang L, Si Y, Yu J, Ding B (2020) In situ Synthesis of Biomimetic Silica Nanofibrous Aerogels with Temperature-Invariant Superelasticity over One Million Compressions. Angew Chem Int Ed 59(21):8285–8292. https://doi.org/10.1002/anie.202001679
31. Guan H, Cheng Z, Wang X (2018) Highly Compressible Wood Sponges with a Spring-like Lamellar Structure as Effective and Reusable Oil Absorbents. ACS Nano 12(10):10365–10373. https://doi.org/10.1021/acsnano.8b05763
32. Su L, Wang H, Niu M, Fan X, Ma M, Shi Z, Guo S-W (2018) Ultralight, Recoverable, and High-Temperature-Resistant SiC Nanowire Aerogel. ACS Nano 12(4):3103–3111. https://doi.org/10.1021/acsnano.7b08577
33. Gao H-L, Zhu Y-B, Mao L-B, Wang F-C, Luo X-S, Liu Y-Y, Lu Y, Pan Z, Ge J, Shen W, Zheng Y-R, Xu L, Wang L-J, Xu W-H, Wu H-A, Yu S-H (2016) Super-elastic and fatigue resistant carbon material with lamellar multi-arch microstructure. Nat Commun 7(1):12920. https://doi.org/10.1038/ncomms12920
34. Zhang X, Cheng X, Si Y, Yu J, Ding B (2022) Elastic and highly fatigue resistant ZrO2-SiO2 nanofibrous aerogel with low energy dissipation for thermal insulation. Chem Eng J 433:133628. https://doi.org/10.1016/j.cej.2021.133628
35. Bhagat SD, Kim Y-H, Ahn Y-S, Yeo J-G (2007) Rapid synthesis of water-glass based aerogels by in situ surface modification of the hydrogels. Appl Surf Sci 253(6):3231–3236. https://doi.org/10.1016/j.apsusc.2006.07.016
36. Xiao Y, Yan M, Shi L, Gong L, Cheng X, Zhang H, Pan Y (2023) High-temperature resistant, super elastic aerogel sheet prepared based on in-situ supercritical separation method for thermal runaway prohibition of lithium-ion batteries. Energy Storage Mater 61:102871. https://doi.org/10.1016/j.ensm.2023.102871